Journal of Applied Electrochemistry **29**: 1217–1227, 1999.

Copper nucleation on titanium for thin film applications

A.J.B. DUTRA and T.J. O'KEEFE
Materials Research Center, University of Missouri-Rolla, Rolla, Missouri 65409-1170, USA

Received 15 June 1998; accepted in revised form 10 November 1998

Key words: copper deposition, copper foil, copper nucleation, electrocrystallization

Abstract

Copper nucleation and growth on titanium substrates from concentrated acidic copper sulfate solutions was studied at 45 and 65 °C and high cathodic potentials. Electrochemical experiments allied to SEM examination were performed to characterize the mechanism of nucleation and its evolution with time. Particular emphasis was given to the influence of potential and agitation on the initial stages of nucleation and growth. Results indicated that most of copper nucleation on titanium from a 83 g dm^{-3} Cu^{2+} solution, at 65 °C, is achieved in a matter of milliseconds. As expected, the initial stages of the copper nucleation and growth is strongly dependent of potential and temperature, and the influence of agitation is only evident at very high potentials. The calculated diffusion coefficients for Cu^{2+} at 45 and 65 °C, under the experimental conditions, were found to be 9.16×10^{-6} and 1.62×10^{-5} cm^2 s^{-1}, respectively.

1. Introduction

The electrochemistry and crystal growth of copper in acidic sulfate solutions has been extensively studied under conditions related to electrowinning and electrorefining [1–7]. However, for the electrolytic production of copper thin films and foil there is considerably less information in the literature.

Although the electrochemical process for foil is basically the same as that for bulk copper production, the conditions and operating parameters are considerably different. In the continuous drum deposition process, the current density, copper concentration and agitation are much higher, while, the sulfuric acid concentration is lower [8–10]. Furthermore, the quality requirements of the product, such as integrity, smoothness as well as mechanical and electrical properties, become much more demanding. As a consequence, initial nucleation and growth of the copper may play a particularly important role in final product quality.

Although copper nucleation on inert substrates has been studied [7, 11–17], the experimental conditions were usually different than those used in the copper foil process. Also, there has been limited attention to the initial stages of the nucleation process, which is fundamental for the production of thin copper foil.

In this study dynamic electrochemical techniques were used to characterize the deposition process at relatively high overpotentials and copper concentrations on a titanium substrate. Finally, the resultant deposits were examined using SEM techniques.

2. Experimental details

2.1. *Deposition system*

The electrochemical cell was a 250 cm^3 jacketed glass beaker with an acrylic cover, which allowed the temperature to remain constant (±0.5 °C) throughout the test. The working electrode was a titanium plate, polished with 600 grit emery paper or a copper foil polished with 0.3 μm alumina, both with an exposed area of 1 cm^2. The counter electrode was an electrolytic copper plate and the reference a Hg/Hg_2SO_4 electrode (+656 mV vs SHE). The electrolyte was prepared from analytical grade cupric sulfate pentahydrate and sulfuric acid to give a stock solution concentration of 83 g dm^{-3} copper and 140 g dm^{-3} sulfuric acid. The electrolyte was not stirred, unless otherwise mentioned, and the temperature was maintained at 45 or 65 °C.

2.2. *Electrochemical tests*

An EG&G PAR model 273A potentiostat/galvanostat connected to a microcomputer with the M270 software was used for the electrochemical tests. All the measurements, unless otherwise mentioned, are referred to the mercury/mercurous sulfate reference electrode. Due to the high ionic strength and temperature of the electrolyte, the solution conductivity was excellent. For this reason there was no *IR* correction made on the polarization curves. Although the curve shapes do not indicate a problem, the variations could become signi-

ficant in the very high current density range and will be further evaluated in the future.

The linear sweep voltammograms on titanium electrodes, at 45 and 65 °C, were started at the open circuit potential (around −260 mV vs Hg/Hg_2SO_4) and driven in the cathodic direction to –1400 mV, all at a scan rate of 1 mV s^{-1}. A similar procedure was carried out with pure copper foil working electrodes, but in this case the equilibrium potential was −350 mV at 45 °C and −335 mV at 65 °C.

The chronopotentiograms were started at the open circuit potential and then stepped to the desired current density, ranging from 350 to 600 mA cm^{-2}, for 45 and 65 °C, in order to estimate the diffusion coefficient of Cu^{2+} under the experimental conditions used in this work. The transition times were measured with the aid of the M270 software, for electrochemical analysis, according to the Kuwana's method, described by Adams [18].

Potentiostatic pulses at different potentials for times of 1 ms to 100 s allied to SEM examination of the copper deposited on the titanium electrodes were the basis of this study. The pulses were provided by the EG&G model 273A potentiostat/galvanostat, which takes about 3 μs to achieve the desired potential. The values of current densities as a function of time, for very short pulses (1 ms) were used to attempt to model the mechanism during the initial stages of nucleation.

3. Results and discussion

3.1. *Electrochemical tests*

Figure 1 shows typical linear sweep voltammograms for copper deposition on titanium electrodes at 45 and 65 °C. A limiting current density region can be observed for potentials more cathodic than about −800 mV up to −1100 mV followed by an increase in the current density at higher potentials. At potentials more cathodic than about –1100 mV a current increase due to hydrogen evolution and rougher surface was observed.

The cathodic branch of Tafel plots for copper deposition on a polished copper foil at 45 and 65 °C is shown in Figure 2. Assuming that the slow step for copper reduction is the discharge of Cu^{2+} to Cu^{+} ions, the transfer coefficient calculated from the Tafel slope for overpotentials between −100 and −200 mV was 0.23 at 45 °C and 0.21 at 65 °C. These values are much lower than those reported by Bockris and Enyo [4], but the Cu^{2+} ion concentration used in this study was at least three times higher than their values. Furthermore, the temperature used in this work was also much higher. The exchange current densities measured from the Tafel plots were found to be 15.7 and 35.7 mA cm^{-2}, at 45 and 65 °C, respectively. Although these numbers are high, they seem to be consistent with an extrapolation of the plot log i_o against log C_{Cu}^{2+}, reported by Slaiman and Lorenz [19].

In Figure 3 typical chronopotentiograms, for copper deposition on titanium, are presented. An initial peak related to copper nucleation followed by a plateau occurred during the first few seconds. This was followed by an increase in cathodic potential, probably due to a mass transport polarization followed by the beginning of hydrogen evolution. A set of chronopotentiograms for different current densities allows the estimation of the Cu^{2+} diffusion coefficient from measured transition times. If Sand's law for a diffusion controlled process is obeyed then the product $i\tau^{1/2}$ is independent of current density and the following relationship is valid:

$$i\tau^{1/2} = \frac{zF\pi^{1/2}C_b D^{1/2}}{2}. \quad (1)$$

Figure 4 shows that Sand's law is satisfied for both temperatures, 45 °C and 65 °C, under these conditions. The calculated diffusion coefficient for Cu^{2+} was 9.16×10^{-6} cm^2 s^{-1} at 45 °C and 1.62×10^{-5} cm^2 s^{-1} at 65 °C. These values are consistent with others

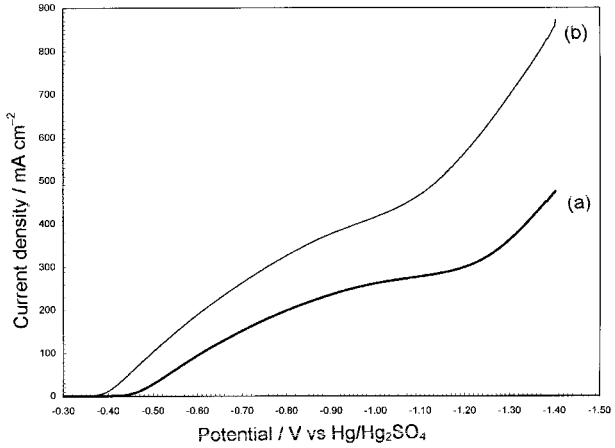

Fig. 1. Cathodic polarization curves for copper deposition on titanium. Temperature: (a) 45 °C and (b) 65 °C. Scan rate 1 mV s^{-1}.

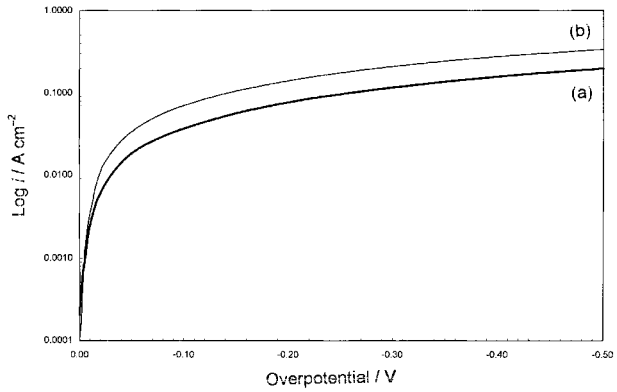

Fig. 2. Tafel plots for copper deposition on copper foil. Temperature: (a) 45 °C and (b) 65 °C. Scan rate 1 mV s^{-1}. Working electrode: polished copper foil.

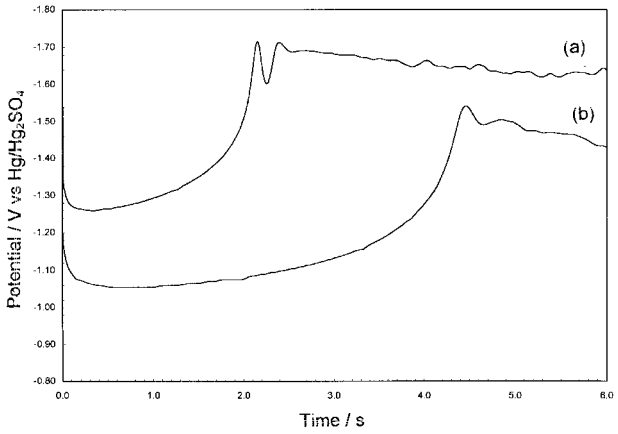

Fig. 3. Typical chronopotentiograms for copper deposition at different temperatures. Temperature: (a) 45 °C and (b) 65 °C. Current density 475 mA cm^{-2}.

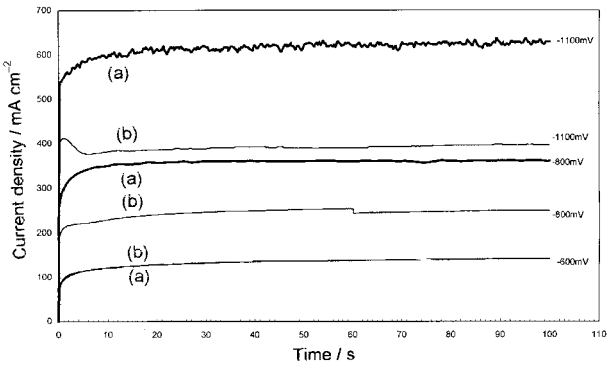

Fig. 5. Effect of magnetic stirring on the current density–time relationship for different potentials at 65 °C. Key: (a) with stirring; (b) no stirring.

previously reported for different conditions, such as 0.95×10^{-5} cm^2 s^{-1}, at 50 °C, for a 50 g dm^{-3} Cu^{2+} and 100 g dm^{-3} sulfuric acid solution [20], 4.88×10^{-6} cm^2 s^{-1}, at 18 °C, for a 25 g dm^{-3} Cu^{2+} and 100 g dm^{-3} H_2SO_4 solution [21], 1.0×10^{-5} cm^2 s^{-1}, at 55 °C, for a 60 g dm^{-3} Cu^{2+}, 140 g dm^{-3} H_2SO_4 and 5 g dm^{-3} Fe solution [22], and 3.82×10^{-6} cm^2 s^{-1}, at 21 °C, for a 0.1M $CuSO_4$, 2 M H_2SO_4 solution [23].

The influence of agitation using a magnetic stirring bar on the potentiostatic pulses at different potentials, for solutions at 65 °C, is shown by the curves in Figure 5. After a sharp rise during the first millisecond, the current remains nearly constant after about 5–10 s of electrolysis, indicating that most of the nucleation occurs in the very beginning of the pulse. At −600 mV, the curves with and without stirring are coincident for 100 s. This is expected because at this potential the current density is under kinetic control as indicated in Figure 1. For more cathodic potentials the effect of stirring becomes clearer as the overpotential is increased beyond –800 mV at 65 °C. At –1100 mV the curve without stirring has a peak at about 1 s, which is probably indicative of diffusion control as it disappears with a moderate magnetic stirring. The current density at this point is in the range normally used in electrolytic copper foil production. The current density is increased nearly 50% with agitation.

The influence of the potential at 65 °C on the current transients during the first millisecond, when most of the nucleation probably occurs, is illustrated in Figure 6. At potentials more cathodic than –900 mV mass transfer limitations began to occur, as indicated by the overlap of the transients for –1100 mV and –900 mV. The effect of magnetic stirring on the beginning of the current transient can be observed in Figure 7. At –600 mV, the curves with and without stirring are coincident, similar to the data presented in Figure 5. At –800 mV, the curves diverged only slightly after about 0.6 ms. Finally, the transients at –1100 mV with and without stirring are very distinct and are completely separated almost immediately showing that growth has a substantial mass transport component.

Thirsk and Harrison [24] have described a straightforward procedure to describe the current density-time relationships for the nucleation and growth of an electrodeposited phase. The derived expressions, shown in Table 1, permit the identification of the nucleation type, growth type and reaction control regime.

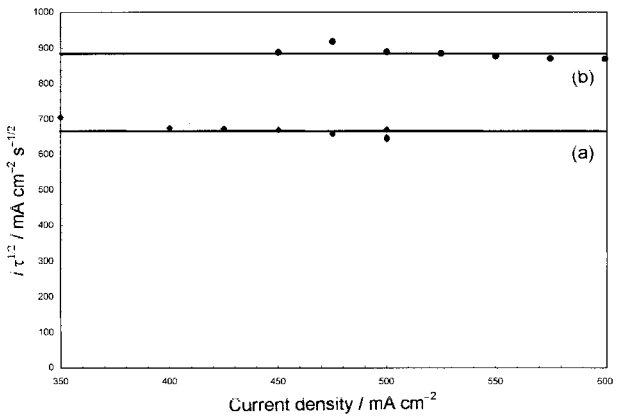

Fig. 4. Validity of Sand's equation for copper reduction at (a) 45 °C and (b) 65 °C.

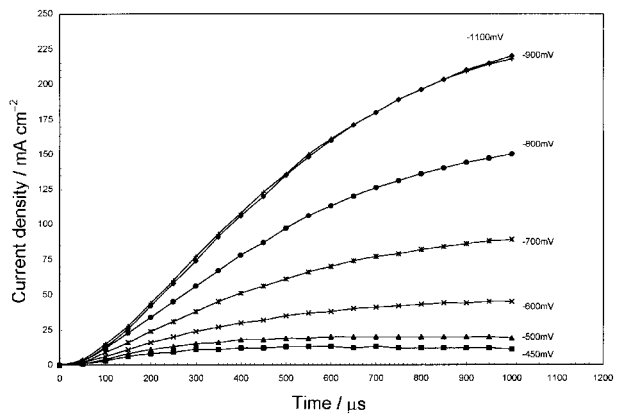

Fig. 6. Influence of the applied potential on current transients for the nucleation of copper on titanium, up to 1 ms, at 65 °C. No stirring.

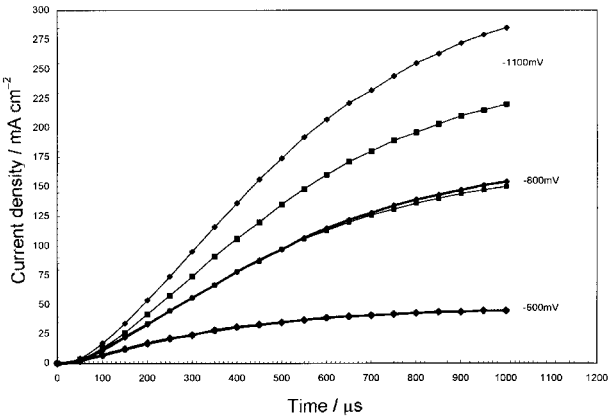

Fig. 7. Influence of magnetic stirring on the potentiostatic current transients for the nucleation of copper on titanium, up to 1 ms, at 65 °C. Key: (◆) with stirring; (■) no stirring.

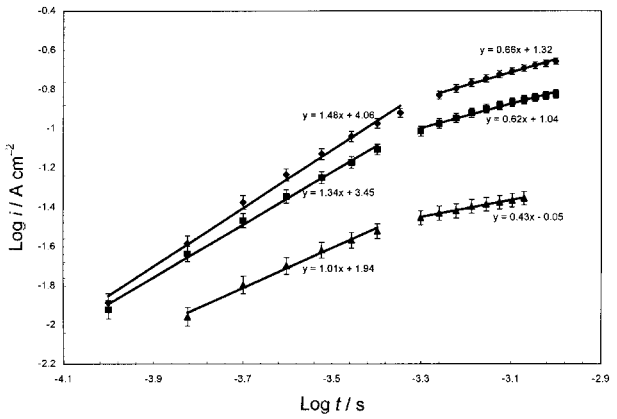

Fig. 8. Logarithmic relationship between current density and time for different potentials at 65 °C, without stirring. Key: (▲) −600 mV; (■) −800 mV; (◆) −1100 mV.

For Equations 2–9 (Table 1), M is the molecular weight of copper (63.54 g mol^{-1}), ρ is the copper density (8.96 g cm^{-3}), D is the diffusion coefficient (cm^2 s^{-1}), C is the concentration of the copper ions (mol cm^{-3}), t is time (s), i is the current density (A cm^{-2}), h the nuclei height, k the reaction rate, L^2 the cross section and θ the coverage. A is defined as $A'N_0$ which is the adjusted nucleation rate constant, A' is the nucleation rate constant and N_0, the total number of sites available for nucleation, which is related with the number of nuclei formed (N) by:

$$N = N_0[1 - \exp(-A't)] \tag{10}$$

The adjusted nucleation rate constant is potentially dependent and can be expressed by

$$A = K\exp(-k\delta^3/\eta^2) \tag{11}$$

where K and k are constants, δ is the surface energy and η the overpotential in mV.

All the expressions presented in Table 1, can be rewritten in a logarithmic form to give

$$\log i = n \log t + \log a \tag{12}$$

where i is the current density in A cm^{-2}, n the power of time and a is a constant that involves the nucleation rate among others factors. If the $\log i - \log t$ plot gives a straight line, the slope is n, which indicates the mechanism of nucleation and a can give an idea of the nucleation rate, assuming that parameters such as the diffusion coefficient, concentration, density and molecular weight are known.

In Figure 8 the $\log i - \log t$ relationship for three different potentials is given, with the vertical error bars indicating an approximate deviation of 2.5% from the straight line model. In the initial time range, the change of the slopes indicates a modification of the nucleation mechanism, from progressive nucleation under kinetic control, at low potential to progressive nucleation under diffusion control, as the cathodic potential is increased. As the time approached 0.5 ms, a slope change was observed, indicating that independently of the potential, the nucleation mechanism can change as the electrodeposition proceeds, even for a very short time. In the second time range the slope values between 0.43 and 0.66, for the different potentials, indicate a diffusion controlled and instantaneous nucleation followed by 3D growth mechanism. However this mechanism in the second time range is hard to be proved by SEM observations, since a progressive nucleation was detected previously.

A summary of the plots shown in Figures 6 and 7 is presented in Table 2. The points before 0.10 ms were not considered in order to avoid interference from double layer charging and possible equipment response delays.

For low cathodic potentials (up to –600 mV) copper nucleation on titanium seems to obey a power depen-

Table 1. Current density–time relationships for potentiostatic nucleation and growth [14, 24]

Expression	Nucleation type	Growth type	Reaction control regime	Equation
$i = 2zFAL^2kt$	progressive	1D needle	kinetic	2
$i = zFh\rho\pi\theta^2DAt/M$	progressive	2D	diffusion	3
$i = 2zF\pi MhN_0k^2t/\rho$	instantaneous	2D	kinetic	4
$i = zF\pi MhAk^2t^2/\rho$	progressive	2D	kinetic	5
$i = 2zF\pi M^2N_0k^3t^2\rho^2$	instantaneous	3D	kinetic	6
$i = 2zF\pi M^2hAk^3t^3/3\rho^2$	progressive	3D	kinetic	7
$i = 8zF\pi N_0M^2C^3D^{3/2}t^{1/2}/\rho^2$	instantaneous	3D	diffusion	8
$i = 16zF\pi AM^2C^3D^{3/2}t^{3/2}/3\rho^2$	progressive	3D	diffusion	9

Table 2. Current–time relationship for the nucleation of copper on titanium at 65 °C

Potential vs. Hg/Hg_2SO_4/ mV	Stirring	Equation and variance for time range 1* (0.10–0.45 ms)	Nucleation mechanism† for range 1
−600	no	$y = 1.01x + 1.94$ $R^2 = 0.99$	1D needle, progressive, kinetic
−700	no	$y = 1.25x + 2.99$ $R^2 = 1.00$	3D, progressive, diffusion‡
−800	no	$y = 1.34x + 3.45$ $R^2 = 1.00$	3D, progressive, diffusion‡
−900	no	$y = 1.43x + 3.93$ $R^2 = 1.00$	3D, progressive, diffusion
−1000	no	$y = 1.47x + 4.01$ $R^2 = 1.00$	3D, progressive, diffusion
−1100	no	$y = 1.48x + 4.06$ $R^2 = 0.99$	3D, progressive, diffusion
−600	yes	$y = 0.91x + 1.60$ $R^2 = 0.99$	2D, instantaneous, kinetic
−800	yes	$y = 1.37x + 3.55$ $R^2 = 0.99$	3D, progressive, diffusion‡
−1100	yes	$y = 1.50x + 4.25$ $R^2 = 1.00$	3D, progressive, diffusion

* $y = \log i$; $x = \log t$

† Refers to growth type, nucleation type and reaction control mechanism

‡ Mixed with 1D needle, progressive and kinetically controlled

dence of time of unity in the range up to 0.45 ms. In this case, it is probably due to a kinetically controlled progressive followed by a needle growth, in accordance with Equation 2. For higher cathodic potentials in this time interval, the mechanism changes gradually to diffusion controlled progressive nucleation followed by 3D growth. At intermediate potentials, between −700 and −800 mV, the nucleation mechanism seems to be a mixture of the mechanisms previously mentioned, since both needle and grainy structures were present, as shown in Figure 9(d). As observed previously [17] for copper nucleation on stainless steel, there appeared to be preferential deposition along the polishing scratches.

3.2. *SEM analysis*

An SEM characterization of various short time deposits of copper on titanium at 65 °C was made and the results are illustrated in Figures 9–13. The influence of potential on copper nucleation morphology after 1 ms, without stirring, is shown in Figure 9. It can be observed that the number of nuclei increases with the increase of cathodic potential, reaching a maximum around –900 mV, when mass transport limitations become evident. At cathodic potentials higher than –900 mV, the number of nuclei remains basically the same, corroborating the potentiostatic transients shown in Figure 6. The different nuclei size characterizes a progressive nucleation mechanism, identified also in the initial time range of the potentiostatic current transients summarized in Table 2. Although different sized nuclei are formed, the distribution range is not wide, which seems to match with a nucleation mechanism change with time from progressive to instantaneous, as indicated in Figure 8. At a higher magnification (3000×), a predominance of a needle-like structure can be observed at lower potentials. This corresponds with the nucleation mechanism proposed in Table 2 for potentials equal or lower than –600 mV. For higher potentials, a morphology of irregularly shaped grains can be observed. These different structures imply a gradual change of the nucleation mechanism as the cathodic potential is increased. Both the needle and grainy structures can be observed on the SEM micrographs but for cathodic potentials higher than –900 mV, very few needles were found. This is consistent with the results for higher potentials presented in Table 2, which indicates a 3D growth, progressive nucleation and diffusion controlled.

The presence of needle type growth is often found at low levels of chloride ion, even in the range of 1 to 5 ppm. Only distilled and deionized water was used in making the solutions because the sensitivity to chloride was recognized. However, there may have been other, inadvertent of chloride ion that could have caused the needle-type nucleation. This issue will be addressed in further studies where the effect of chloride ion concentration is evaluated.

The evolution of the copper nuclei with time at −600 mV, 65 °C, without stirring is presented in Figure 10. It can be observed that the number of nuclei does not change appreciably after 1 ms, indicating that most of the nucleation occurs during this period of time. After that, the growth of the copper dominates and the needle shape observed initially tends to disappear. The copper crystals then form multifaceted 3D agglomerates which continue to merge with neighbours until near complete electrode surface coverage. This process indicates the presence of zones of excluded nucleation, described by Markov [25] and Kovarskii and Arzhanova [26], which preclude the formation of new nuclei in the zone of influence of previously formed nuclei. Then, after the formation of a determinate number of nuclei, growth should be the predominant process. Similar behavior is shown in Figure 11, for the copper nucleation and growth at –800 mV, without stirring. The main difference is that the number of nuclei after 1ms is much greater for –800 mV and after 100 s, when the electrode surface is almost completely covered, the copper deposit has a finer structure. Additionally, the needle shaped appearance tends to disappear faster at –800 mV.

The effect of agitation using a magnetic stirring bar on copper nucleation and growth at –800 mV and 65 °C is shown in Figure 12. After 1 ms, no significant difference was observed for the copper nucleation with and without stirring, as should be expected, since there is little effect of stirring on the current transients at –800 mV, shown in Figure 7. Nevertheless, it could be

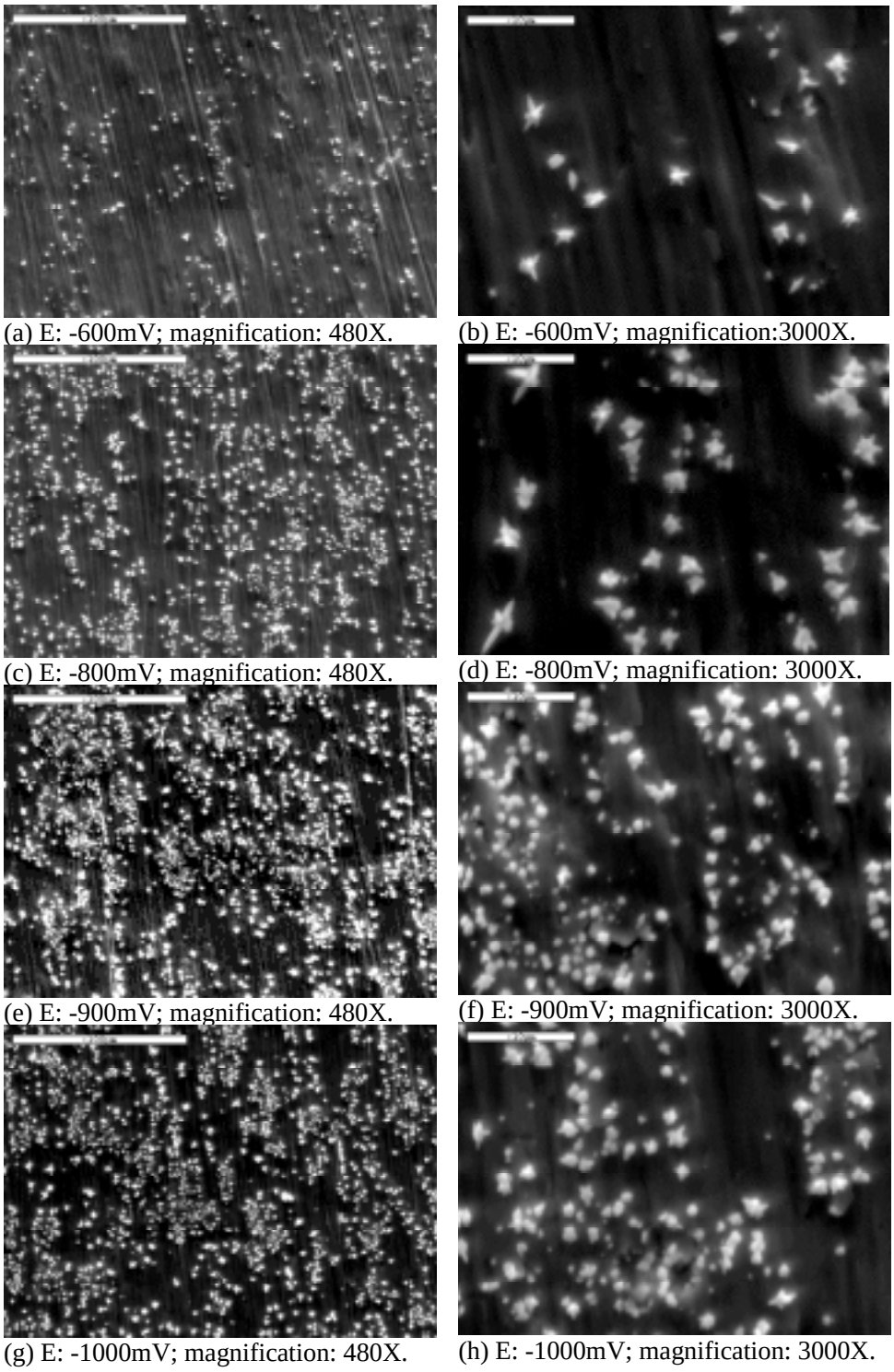

Fig. 9. SEM micrographs of copper nuclei obtained at different potentials, without stirring, after 1 ms.

observed that stirring does affect copper growth, and the copper grains obtained after 100 ms with stirring are much more uniform and do not present needle-like crystals. After 20 s, the copper grains in the stirred electrolyte are larger and more homogeneous than without stirring. Finally, after 100 s, the copper structure seemed to be smoother than that obtained without stirring. These observations are in agreement with the potentiostatic current transients at –800 mV, given in Figures 5 and 7. Agitation had no effect on the apparent current density during the initial nucleation stage, but with times in the range of 10 to 100 s there was about a 50% increase in current density with stirring.

The effect of stirring on copper nucleation and growth at –1100 mV and 65 °C is shown in Figure 13. A clear modification on the nuclei shape can be observed for Figure 13(a) and (b), after 1 ms, since with stirring the

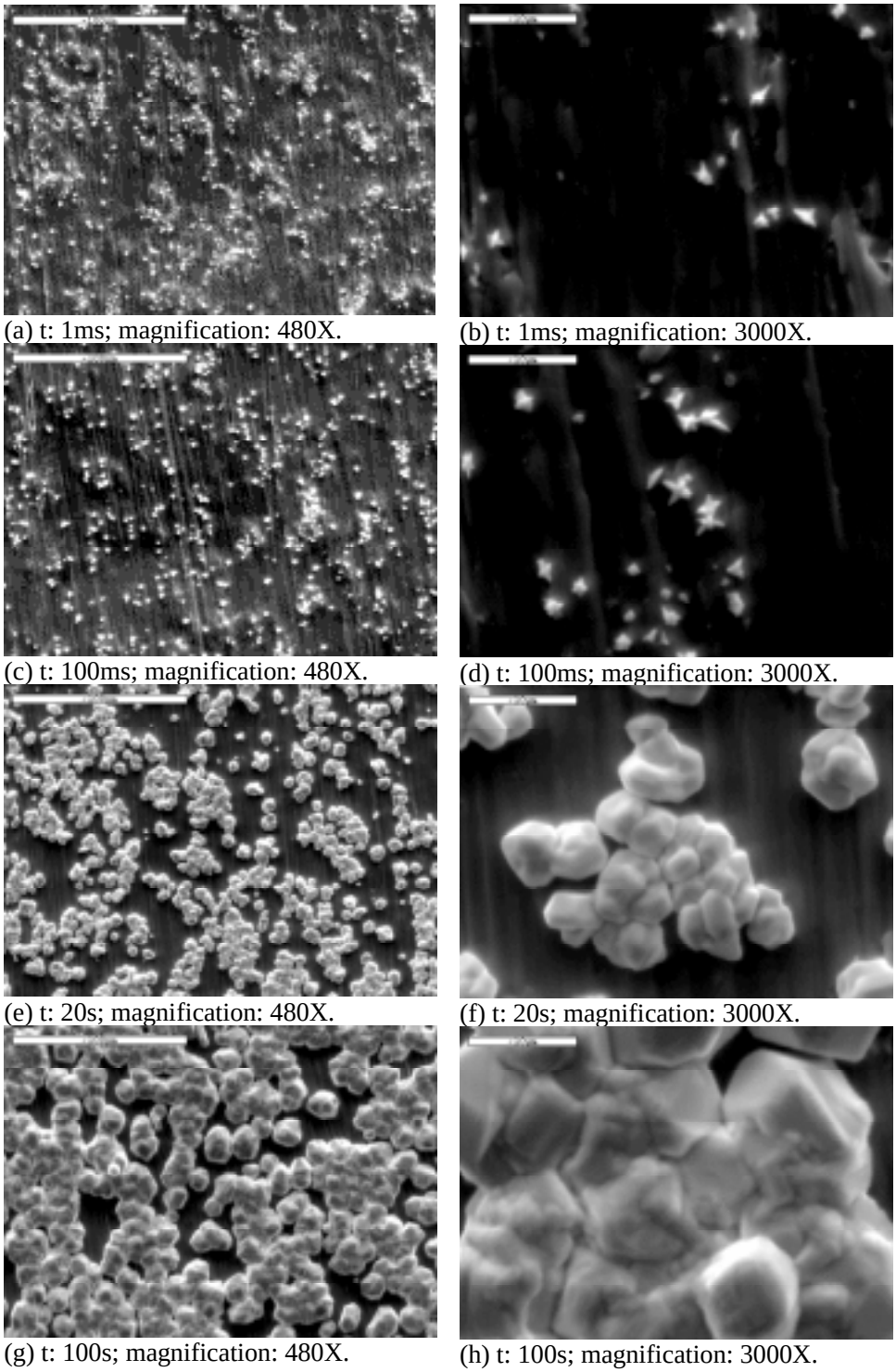

Fig. 10. SEM micrographs of copper crystals obtained at −600 mV vs Hg/Hg_2SO_4, without stirring, after different times.

nuclei shape and size were more uniform and no needles were observed anymore. Furthermore, at 480 × magnification, it can be observed that without stirring the number of nuclei after 1 ms is greater and their size slightly smaller than with stirring. This behaviour should be expected since for progressive nucleation under diffusion control the current is concentrated in the initially formed nuclei. Consequently the higher current levels attained due to stirring, the zones of excluded nucleation may become larger, leading to a smaller number of nuclei but with increased size. After 100 s the electrode surface was completely covered in both cases, but the copper structure obtained without stirring was rougher and already presented some indication of preferential growth that could lead to dendrite formation. The use of a moderate magnetic agitation was not sufficient to change the proposed mechanism of nucleation, exhibited in Table 2, but obviously strongly

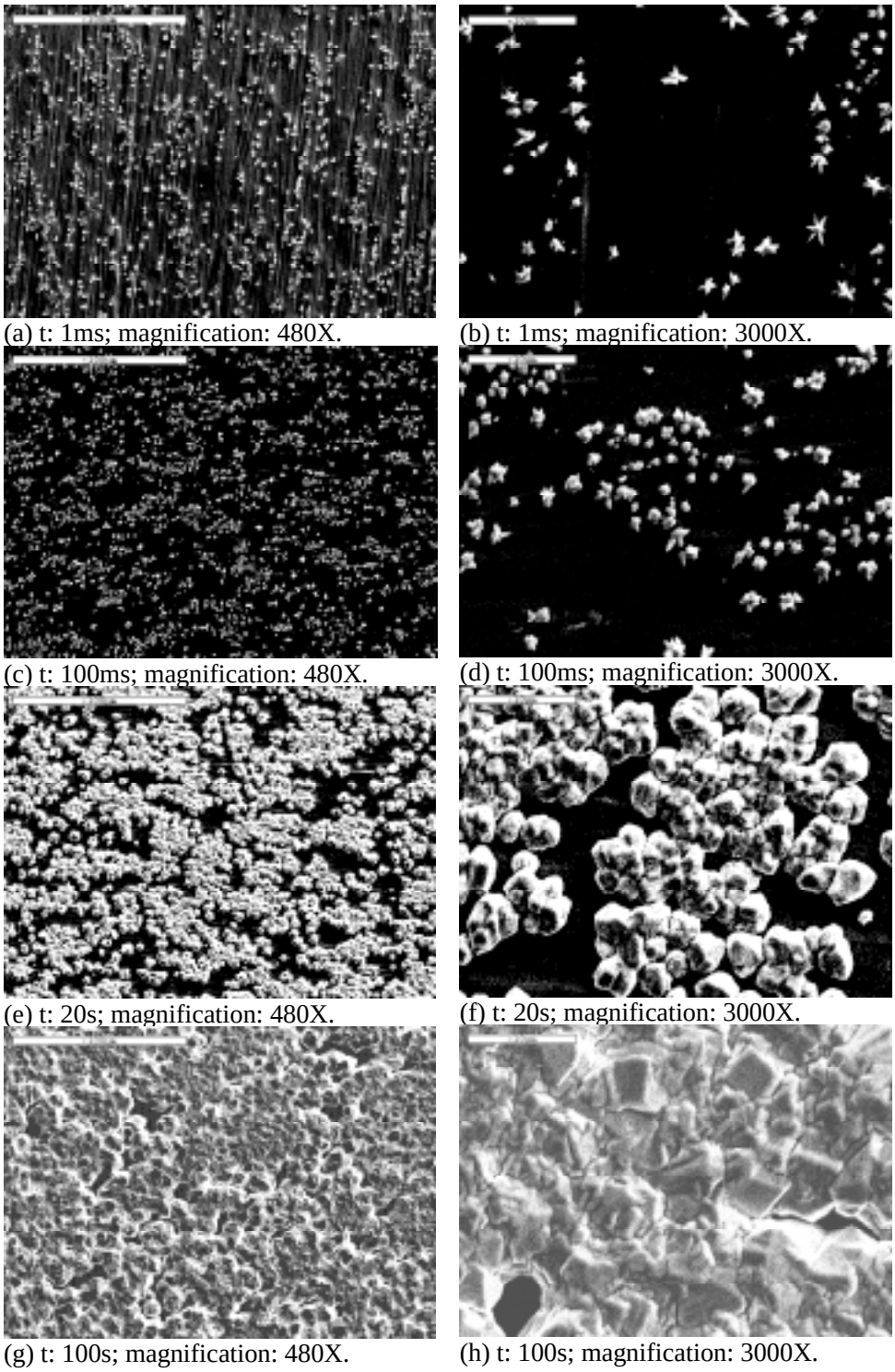

Fig. 11. SEM micrographs of copper crystals obtained at −800 mV vs Hg/Hg_2SO_4, without stirring, after different times.

affects the copper nuclei morphology and growth rate, as the current density is increased with stirring.

The SEM micrographs have shown that the saturation nucleus density is strongly potential dependent and, at least for high temperatures and copper concentration, the saturation is reached after a few milliseconds of electrolysis. The higher the cathodic potential the higher is the saturation nucleus density because the number of active sites taking part in the nucleation process will be greater. These features are in accordance with the theory of saturation nucleus density described by Markov [25].

It is recognized that the initial surface condition of the titanium cathode can also have a major, often dominating, effect on the copper nucleation and growth. The surface treatment was constant during this study but additional tests are planned to identify the influence of surface on nucleation.

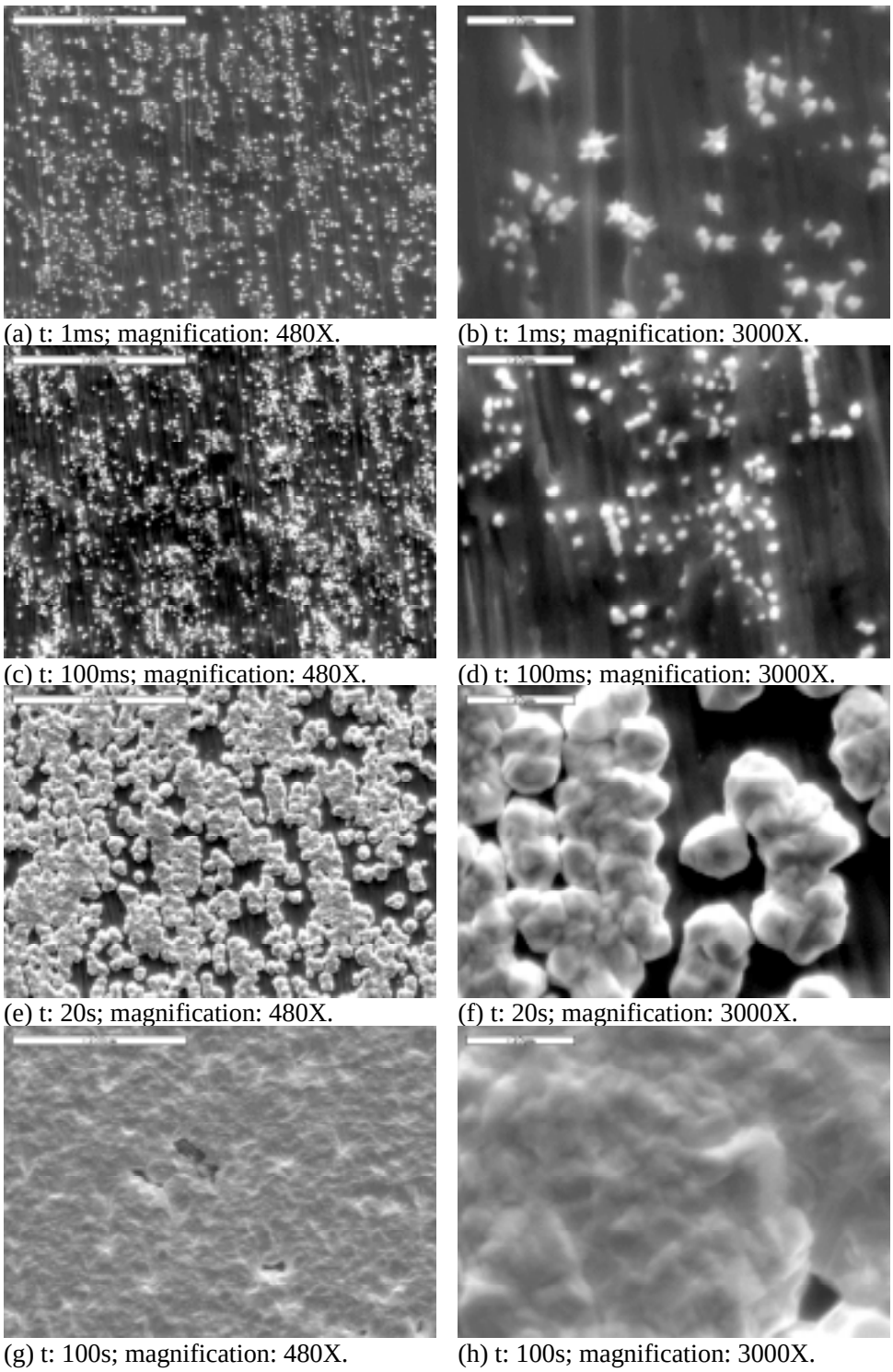

Fig. 12. SEM micrographs of copper crystals obtained at −800 mV vs Hg/Hg_2SO_4, with stirring, after different times.

4. Conclusions

The following conclusions can be drawn from the above investigation:

(i) The agreement between theory, electrochemical tests and SEM observations is quite good and allowed an indication of the mechanism of copper nucleation on titanium using relatively concentrated solutions at elevated temperatures.

(ii) The saturation nucleus density is strongly potential dependent, increasing with increasing cathodic potentials up to about –900 mV, when mass transport limitations begin to affect the initial stage of nucleation.

(iii) In the lower potential range the initial mechanism of copper nucleation seems to be progressive nucleation, 1D needle growth and diffusion controlled. In the higher potential range (below

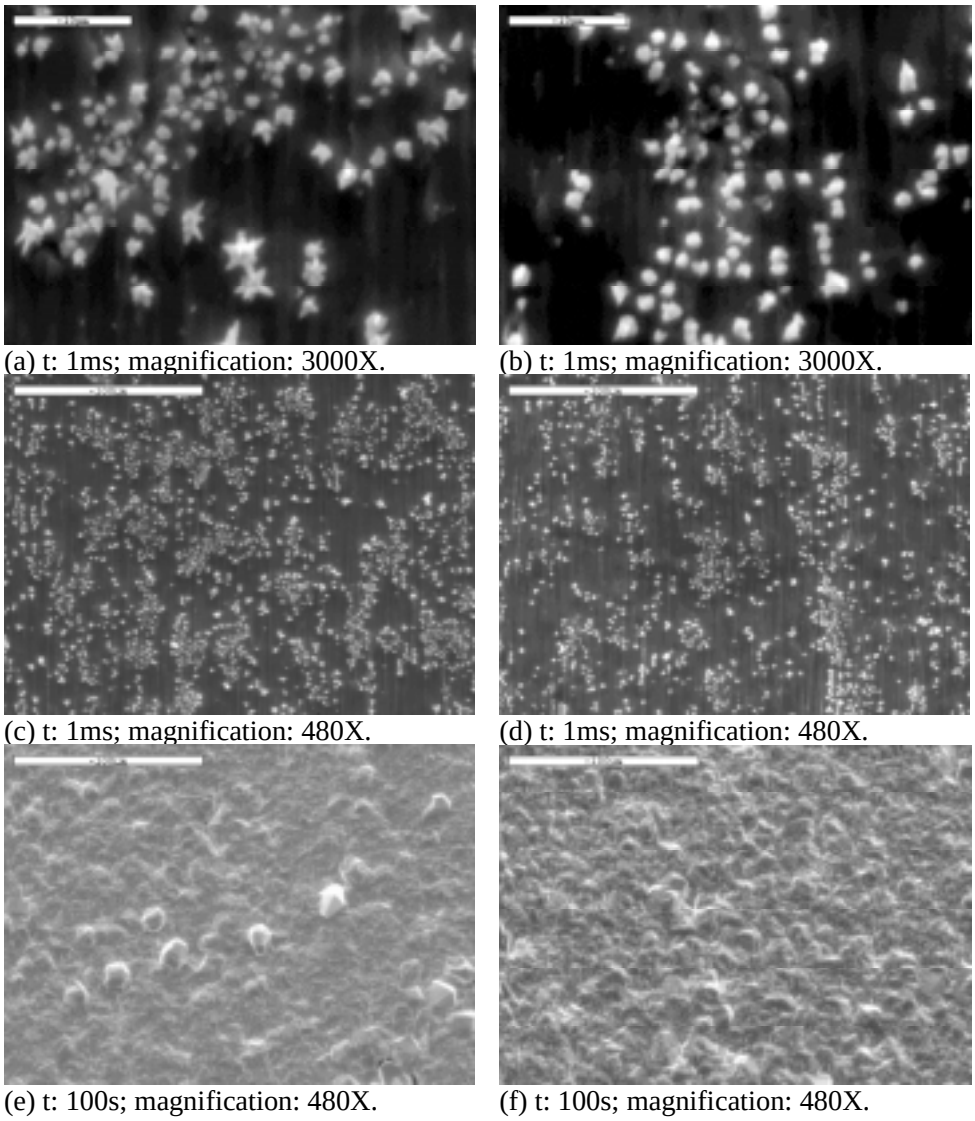

Fig. 13. SEM micrographs of copper crystals obtained at −1100 mV vs Hg/Hg_2SO_4, after different times. (a), (c) and (e) without stirring and (b), (d) and (f) with stirring.

−700 mV) it seems to be progressive nucleation, 3D growth and diffusion controlled, although there is not a clear potential value for this change.

(iv) The mechanism of nucleation seems to change after a short time period to instantaneous, diffusion controlled and followed by 3D growth.

(v) The saturation nucleus density is achieved in a very short period of time, often in a matter of milliseconds, in the potential range tested. No continued significant nucleation was observed after a few milliseconds and the morphology study showed a clear lateral growth of the nuclei initially formed with time.

(vi) Agitation affects the initial nucleation only at very high cathodic potentials, leading to a slightly larger and more homogeneous nuclei size and finally to a smoother copper deposit.

(vii) The calculated diffusion coefficients for Cu^{2+} at 45 and 65 °C, under the experimental conditions, were found to be 9.16×10^{-6} and 1.62×10^{-5} $cm^2\ s^{-1}$, respectively.

Acknowledgements

One of the authors (AJBD) is grateful to CNPq (Brazilian Research Council) for the one year grant as Post-doctoral fellow and to the Federal University of Rio de Janeiro for the license, allowing him to perform research at the University of Missouri–Rolla.

References

1. R.C. Turner and C.A. Winkler, *J. Electrochem. Soc.* **99** (1952) 78.
2. J.O'M. Bockris and B.E. Conway, *J. Chem. Physics* **28** (1958) 707.

3. E. Mattsson and J.O'M. Bockris, *Trans. Faraday Soc.* **55** (1959) 1586.
4. J.O'M. Bockris and M. Enyo, *Trans. Faraday Soc.* **58** (1962) 1187.
5. N. Ibl and K. Schadegg, *J. Electrochem. Soc.* **114** (1967) 54.
6. V.A. Ettel, A.S. Gendron and B.V. Tilak, *Metall. Trans.* **6B** (1975) 31.
7. H. Sun, J.L. Delplanke, R. Winand and T.J. O'Keefe, *in* 'Copper 91 – Cobre 91 International Symposium', vol. III, edited by W.C. Cooper, D.J. Kemp, G.E. Lagos and K.G. Tan, TMS, Ottawa (1991), p. 405.
8. S.J. Clouser, D.F. Franco and C.J. Hasegawa, *US Patent 5 421 985* (6 June 1995).
9. R.D. Apperson, S.J. Clouser and R.D. Patrick, *US Patent 5 403 465* (4 Apr. 1995).
10. A.J. Brock, L. Lin P. Menkin and N.W. Polan, *US Patent 5 181 770* (26 Jan. 1993).
11. G. Gunawardena, G. Hills and I. Montenegro, *J. Electroanal. Chem.* **184** (1985) 357.
12. J-L. Delplancke, M. Sun, T.J. O'Keefe and R. Winand, *Hydrometall.* **23** (1989) 47.
13. J-L. Delplancke, M. Sun, T.J. O'Keefe and R. Winand, *Hydrometall.* **24** (1990) 179.
14. M. Sun and T.J. O'Keefe, *Metall. Trans.* **23B** (1992) 591.
15. M. Urda, L. Oniciu, J-L. Delplancke and R. Winand, *J. Appl. Electrochem.* **27** (1997) 616.
16. J. Zhang, K. Teng and T.J. O'Keefe, *Surf. Coat. Technol.* **89** (1997) 225.
17. Z. Zhou and T.J. O'Keefe, *J. Appl. Electrochem.* **28** (1998) 461.
18. R.N. Adams, 'Electrochemistry at Solid Electrodes' (Marcel Dekker, New York, 1969), p. 183.
19. Q.J.M. Slaiman and W.J. Lorenz, *Electrochim. Acta* **19** (1974) 791.
20. H.M. Wang, S.F. Chen, T.J. O'Keefe, M. Degrez and R. Winand, *J. Appl. Electrochem.* **19** (1989) 174.
21. T.J. O'Keefe, J.S. Cuzmar and S.F. Chen, *J. Electrochem. Soc.* **134** (1987) 547.
22. V.A. Ettel, B.V. Tilak and A.S. Gendron, *J. Electrochem. Soc.* **121** (1974) 867.
23. R. Caban and T.W. Chapman, *J. Electrochem. Soc.* **124** (1977) 1371.
24. H.R. Thirsk and J.A. Harrison, 'A Guide to the Study of Electrochemical Kinetics' (Academic Press, New York, 1972), p.118.
25. I. Markov, *Thin Solid Films* **35** (1976) 11.
26. N. Ya. Kovarskii and T.A. Arzhanova, *Elektrokhimiya* **22** (1986) 452.